Inorganic Chemistry

Article

pubs.acs.org/IC

Intramolecular Oxyl Radical Coupling Promotes O–O Bond Formation in a Homogeneous Mononuclear Mn-based Water Oxidation Catalyst: A Computational Mechanistic Investigation

Douglas W. Crandell,[†] Song Xu,[†] Jeremy M. Smith,*[,†] and Mu-Hyun Baik*[,‡,§]

[†]Department of Chemistry, Indiana University, 800 East Kirkwood Avenue, Bloomington, Indiana 47405, United States
[‡]Institute for Basic Science (IBS), Center for Catalytic Hydrocarbon Functionalizations, Daejeon, 34141, South Korea
[§]Department of Chemistry, Korea Advanced Institute of Science and Technology (KAIST), Daejeon, 34141, South Korea

Supporting Information

ABSTRACT: The mechanism of water oxidation performed by a recently discovered manganese pyridinophane catalyst $[Mn(Py_2N^tBu_2)(H_2O)_2]^{2+}$ is studied using density functional theory methods. A complete catalytic cycle is constructed and the catalytically active species is identified to consist of a Mn^V-bis(oxo) moiety that is generated from the resting state by a series of proton-coupled electron transfer reactions. Whereas the electronic ground state of this key intermediate is found to be a triplet, the most favorable pathway for O–O bond formation is found on the quintet potential energy surface and involves an intramolecular coupling of two oxyl radicals with opposite spins bound to the Mn-center that adopts an electronic structure most consistent formally with a high-spin Mn^{III} ion. Therefore, the thermally accessible high-spin quintet state that constitutes a typical and innate property of a first-row transition metal center plays a critical role for catalysis. It enables facile electron transfer between the oxo moieties and the Mn-center and promotes O–O bond formation via a radical coupling reaction with a calculated reaction barrier of only 14.7 kcal mol^{-1}. This mechanism of O–O coupling is unprecedented and provides a novel possible pathway to coupling two oxygen atoms bound to a single metal site.

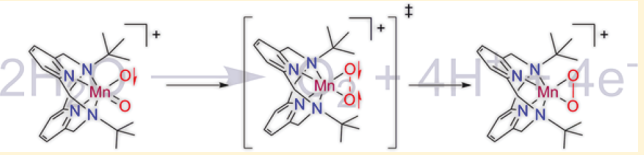

INTRODUCTION

Oxidizing water to harvest electrons for the reduction of carbon dioxide into more useful commodity chemicals is a key technology for the abatement of our current dependence on fossil fuels and for reducing, if not eliminating, the production of atmospheric greenhouse gases.[1−4] Since the report of the "blue dimer",[5] one of the first homogeneous water oxidation catalysts, significant efforts have been made in developing water oxidation catalysts;[6] systems based on multiple metal centers inspired by the Mn_4CaO_5 cluster in the oxygen-evolving complex (OEC) of Photosystem II have received much attention.[7,8] Particularly interesting are catalysts based on earth-abundant first-row transition metals, especially manganese, as it features in both the OEC and the active site of another oxygen-evolving enzyme, manganese catalase.[9−11] The current limited understanding of the mechanism of O_2 evolution in the OEC[12−14] has slowed the development of synthetic Mn-based catalysts that mimic the mechanism of these natural systems.[6,15] There have been a few reports of stoichiometric production of O_2 from water or hydroxide using Mn-based systems.[16,17] Catalytic O_2 evolution[18−23] can be achieved in the presence of water using chemical oxidants.[24−29] Electrocatalytic O_2 production has also been demonstrated typically in nonaqueous solvents.[21,30,31] The robustness of these catalysts under standard reaction conditions often poses a significant challenge for identifying compounds that are truly molecular catalysts, rather than being precursors for nanoparticles or heterogeneous catalysts that are active for O_2 evolution.

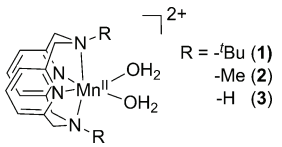

Figure 1. Structures of complexes **1**, **2**, and **3**.

One of us recently reported a stable, homogeneous catalyst based on an pyridinophane macrocycle $[Mn(Py_2N^tBu_2)(H_2O)_2]^{2+}$ (**1**) for electrocatalytic water oxidation in aqueous solution at pH 12.2.[32] Previous studies suggest that the catalyst is mononuclear and that switching the alkyl substituents from Me (**2**) or H (**3**) on the amino groups to *tert*-butyl changes the catalyst activity from hydrogen peroxide disproportionation to water oxidation. It was hypothesized that these large substituents prevent the formation of catalytically inactive manganese dimers. Mechanistic studies also showed that proton-transfer from the aqua ligands accompanies complex oxidation,[33] suggesting that the ligand framework can potentially support high-valent metal-oxo intermediates postu-

Received: December 29, 2016
Published: April 4, 2017

DOI: 10.1021/acs.inorgchem.6b03144
Inorg. Chem. 2017, 56, 4435−4445

lated to be responsible for forming the O−O bond. On the basis of the first-order dependence of the rate on catalyst concentration and electrochemical studies, it was proposed that O−O bond formation proceeded through nucleophilic attack of H_2O/OH^- on a high-valent manganese oxo species.[32]

Understanding how this challenging reaction couples two oxygen atoms that are formally in a −II oxidation state is imperative for developing rational design strategies for improved catalysts. In the OEC, oxyl radical intermediates have been proposed to be necessary for O−O bond formation.[34−38] Similar electronic structures demonstrating redox noninnocence of the oxo fragment have been found for the formally Ru^V═O fragment of the "blue dimer".[39] Recently we have shown that a mononuclear Co-based catalyst is able to generate a biradicaloid oxene fragment with a formal oxidation state of zero that is remarkably reactive toward hydroxide in basic solution. This unusual electronic structure is facilitated by the accessibility of the high-spin state, which enables significant electron transfer from the oxo moiety into the half-filled Co−dπ orbitals of the highly electropositive metal center.[40] Intrigued as to whether other first-row transition-metal catalysts possess other unusual electronic structures, or perhaps similar ones that are ultimately responsible for water oxidation, this work investigates how a single manganese ion supported by an aminopryidine macrocycle and featuring two oxygen-based ligands in a *syn*-configuration may facilitate O_2 evolution.

COMPUTATIONAL DETAILS

All calculations were performed using density functional theory[41,42] as implemented in the Jaguar 8.1 suite of ab initio quantum chemistry programs.[43] Geometry optimizations were performed with the M06 functional using the 6-31G** basis set.[44−48] Mn was represented using the Los Alamos LACVP basis set that includes relativistic core potentials.[49−51] More accurate single point energies were computed from the optimized geometries using Dunning's correlation-consistent triple-ζ basis set, cc-pVTZ(-f) that includes a double set of polarization functions.[52] Mn was represented using a modified version of LACVP, designated as LACV3P, in which the exponents were decontracted to match the effective core potential with triple-ζ quality. Vibrational frequencies were computed at the M06/6-31G** level of theory to derive zero point energy and vibrational entropy corrections from unscaled frequencies. Entropy here refers specifically to the vibrational/rotational/translational entropy of the solutes, as the continuum model includes the entropy of the solvent. All intermediates were confirmed as local minima on the potential energy surface having zero imaginary frequencies. Transition states were confirmed to possess only one imaginary frequency. Solvation energies were evaluated using a self-consistent reaction field (SCRF) approach based on accurate numerical solutions of the linearized Poisson−Boltzmann equation.[53−56] Solvation calculations were carried out on the optimized gas-phase geometries using a dielectric constant of ε = 80.37 for water and ε = 37.5 for acetonitrile. As with all continuum models, the solvation energies are subject to empirical parametrization of the atomic radii that are used to generate the solute surface. We employ the standard set of optimized radii in Jaguar for H (1.150 Å), C (1.900 Å), N (1.600 Å), O (1.600 Å), and Mn (1.480 Å). Antiferromagnetic states were modeled using Noodleman's broken symmetry (BS) formalism without spin projection.[57−59] The change in solution phase free energy $\Delta G(\mathrm{sol})$ was calculated as follows:

$$\Delta G(\mathrm{sol}) = \Delta G(\mathrm{gas}) + \Delta\Delta G_{\mathrm{solv}} \quad (1)$$

$$\Delta G(\mathrm{gas}) = \Delta H(\mathrm{gas}) - T\Delta S(\mathrm{gas}) \quad (2)$$

$$\Delta H(\mathrm{gas}) = \Delta E(\mathrm{SCF}) + \Delta\mathrm{ZPE} \quad (3)$$

$\Delta G(\mathrm{gas})$ is the change of free energy in gas phase; $\Delta\Delta G_{\mathrm{solv}}$ = change in free energy of solvation; $\Delta H(\mathrm{gas})$ = change in gas phase enthalpy; T = temperature (298.15 K); $\Delta S(\mathrm{gas})$ = change in gas phase entropy; $\Delta E(\mathrm{SCF})$ = self-consistent field energy, that is, "raw" electronic energy as computed from the SCF procedure at the triple-ζ level; ΔZPE = change in vibrational zero point energy.

For computations involving proton-coupled redox reactions it is necessary to account for the free energy of a proton in solution. We used the following expression to compute $G(H^+)$, the free energy of a proton in solution

$$G(H^+) = H^{\mathrm{gas}}(H^+) - TS + \frac{5}{2}RT + G_{\mathrm{solv}}(H^+) \quad (4)$$

where $H^{\mathrm{gas}}(H^+)$, the gas-phase electronic energy, is zero by definition; R is the gas constant; T is 298.15 K; S is the translational entropy of a free hydrogen atom calculated using the Sackur−Tetrode equation (26.04 eu); 5/2 RT is the thermal correction, which amounts to 0.064 eV at 298.15 K; and $G_{\mathrm{solv}}(H^+)$ is the free energy of solvation of a proton (−265.9 kcal mol^{-1}).[60,61] Since experimental redox potentials are measured at pH 12.2, our computed standard redox potentials were adjusted to the experimental pH conditions using the Nernst equation:

$$E_{1/2}(\mathrm{calcd})_{\mathrm{pH}} = E_{1/2}(\mathrm{calcd}) - RT\ln(10)/n_e \times n_{H+} \times \mathrm{pH} \quad (5)$$

where n_e and n_{H+} are the numbers of electrons and protons, respectively. The value of RT is computed to be 0.0257 V at 298.15 K; thus, according to the above equation, ~0.72 V should be subtracted from the computed standard redox potentials when one proton is involved in the redox reaction at pH 12.2. Reaction energies are calculated as follows:

$$\Delta G(\mathrm{sol})_{\mathrm{rxn}} = \Delta G(\mathrm{sol})_{\mathrm{products}} - \Delta G(\mathrm{sol})_{\mathrm{reactants}} \quad (6)$$

To account for the energy required to generate a hydroxide ion at pH 12.2, an additional 0.72 V (16.6 kcal mol^{-1}) is added to the energies of any intermediates or transition states involving the direct addition of hydroxide (i.e., not through the stepwise addition of water). Coordinates of all calculated structures, vibrational frequencies, and calculated energy components are available in the Supporting Information.

RESULTS AND DISCUSSION

For our computational analysis to properly select intermediates that are most relevant for the water oxidation mechanism, it is important to benchmark our calculations against experimental observables. The complex was crystallographically characterized as the acetonitrile solvate $[Mn^{II}(Py_2N^tBu_2)(ACN)_2]^{2+}$ **4**.[32] The ground state of this Mn(II)-d^5 complex **4** is calculated to be the high-spin (HS) sextet state, which is 37.1 kcal mol^{-1} lower in energy than the low-spin (LS) alternative, quartet state. Figure 2 shows the optimized structure of the sextet complex ^{6}**4** and

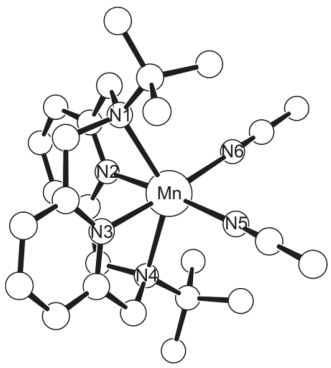

Figure 2. Optimized structure of ^{6}**4**. Hydrogen atoms are omitted for clarity.

DOI: 10.1021/acs.inorgchem.6b03144
Inorg. Chem. 2017, 56, 4435−4445

the most pertinent bond lengths and angles are compared to those of the previously reported X-ray crystal structure in Table 1. The structural parameters of the DFT optimized structure

Table 1. Select Bond Lengths in Å and Angles in deg for Crystal and Optimized Structures of ^{6}4

	experimental[32]	computed
Mn−N1	2.455	2.460
Mn−N2	2.165	2.172
Mn−N3	2.236	2.167
Mn−N4	2.415	2.467
Mn−N5	2.152	2.303
Mn−N6	2.211	2.303
N1−Mn−N4	143.4	137.4

are in good agreement with those found in the crystal structure with most of the computed bond lengths being slightly longer than the experimental values. It is well established that density functional calculations tend to yield slightly expanded structures with overestimated bond lengths in transition metal complexes.[62]

The geometry of ^{6}**4** provides a useful benchmark for modeling the Mn^{II} high-spin (HS) resting state for the catalytic cycle. But a key question is what the nature of the intermediate responsible for O−O bond formation maybe is it formally a Mn^{IV}═O or a Mn^{V}═O species? Both have been proposed to be relevant for water oxidation.[8,34−38,63,64] Because these high-valent oxo intermediates are highly reactive, they are often fleeting intermediates during catalysis making them difficult to study experimentally. Previously, we showed that redox potentials for transition metal complexes can be successfully approximated using density functional calculations[65] and theoretical models of proton-coupled electron transfer reactions are well established.[66,67] Thus, our quantum chemical models constitute a reasonable platform for investigating which reactive species should predominate in solution following electrochemical oxidation. The cyclic voltammogram of $[Mn^{II}(Py_2N^tBu_2)(H_2O)_2]^{2+}$ **1** at pH 12.2 in aqueous solution displays a Faradaic response at ca. 1.0 V along with a large irreversible wave that has an onset potential of approximately 1.3 V and a peak potential at about 1.5 V.[32] Because our calculations produce standard potentials, they should not match these experimental peak potentials.[68] But the experimental peak potential can be expected to serve as an upper limit for the standard potentials calculated assuming different redox-active species.

Scheme 1 illustrates the relative energies of postulated electrochemical intermediates that may be formed en route to generating a high-valent metal-oxo species at pH 12.2. The removal of electrons is shown with vertical arrows as the associated standard potential vs normal hydrogen electrode (NHE) for each oxidation process. Deprotonation energies are visualized in the horizontal direction. The calculated pK_a value for each intermediate is listed in red on top of the horizontal arrow with the corresponding pH-adjusted Gibbs free energy for the deprotonation event given below the arrow in black. The diagonal arrows then correlate with the removal of both a proton and electron in concert as a proton-coupled electron transfer (PCET) event. For the initial Mn^{II} complex **1**, the sextet state ^{6}**1** is favored over the quartet by 46.0 kcal mol^{-1}. The pK_a of one of the aqua protons on ^{6}**1** is calculated to be 11.35, which at pH 12.2 suggests that the equilibrium between ^{6}**1** and ^{6}**5** should slightly favor the latter with ^{6}**5** being 1.2 kcal mol^{-1} more favorable in terms of ΔG(sol).

Oxidation of the dicationic ^{6}**1** requires 1.561 V vs NHE, but removal of an electron from ^{6}**5** needs only −0.128 V vs NHE as the initial removal of a proton allows for avoiding excessive charge buildup around the metal center. The resulting Mn^{III} ion in ^{5}**8** adopts a HS configuration, as the quintet state is favored over the triplet state by 33.0 kcal mol^{-1}. Our calculations indicate that ^{5}**8** will rapidly deprotonate and generate the Mn^{III}-bis(hydroxyl) species ^{5}**9** given the calculated pK_a of 1.59—therefore, we do not expect ^{5}**8** to be detectable experimentally,

Scheme 1. Relative Solution-Phase Free Energies of Potential Electrochemical Intermediates

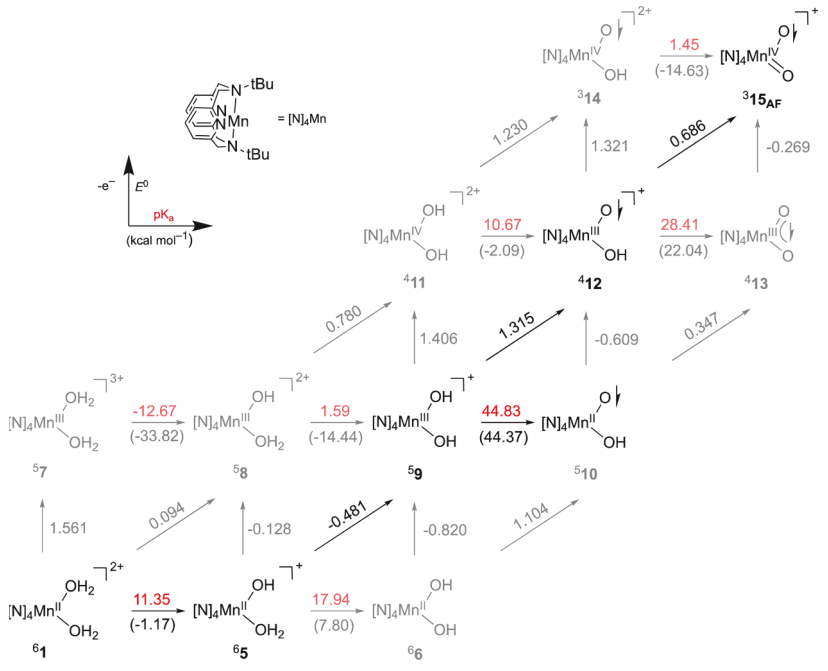

DOI: 10.1021/acs.inorgchem.6b03144
Inorg. Chem. 2017, 56, 4435−4445

as illustrated in gray in Scheme 1. The ease of deprotonation of ^{5}**8** indicates that the removal of the electron and proton should occur in a concerted fashion as a PCET, which is calculated to have an overall standard potential of −0.481 V vs NHE. The alternative $[Mn^{III}(Py_2N^tBu_2)(O)\ (OH_2)]^+$ complex ^{5}**9A** was also examined, but the quintet state for this isomer was found to be 37.2 kcal mol^{-1} higher in energy than ^{5}**9**, disqualifying it from being mechanistically relevant.

Removal of a proton from ^{5}**9** is prohibitively high in energy, requiring 44.4 kcal mol^{-1}. The removal of a single electron to give ^{4}**11** is calculated to require 1.406 V vs NHE, whereas coupling the removal of the electron with a proton should proceed at a more negative potential of 1.315 V vs NHE to produce ^{4}**12**. The bis(hydroxyl) species ^{4}**11** is 6.8 kcal mol^{-1} lower in energy than the $[Mn^{IV}(Py_2N^tBu_2)(O)(OH_2)]^{2+}$ intermediate ^{4}**11A**. Species ^{4}**12** contains formally a $[Mn^{IV}{=}O]^+$ fragment, the electronic structure of which can be better described using the resonance form $[Mn^{III}{-}O^{\bullet}]^+$ based on Mulliken spin density analysis that assigns an excess α-spin density of 3.60 on Mn and excess β-spin density of 0.71 on the oxo moiety. This spin distribution is most consistent with a HS Mn^{III} ion that is antiferromagnetically (AF) coupled to an oxyl radical ligand. The sextet ^{6}**12** featuring a HS Mn^{III} center (Mulliken spin density of 3.90α) and an oxyl radical fragment with a parallel Mulliken spin population 1.01α was found to be 15.5 kcal mol^{-1} above the quartet state. The doublet state was located at an even higher 22.0 kcal mol^{-1} above the ground state quartet. Our calculations indicate that an additional PCET from ^{4}**12** to yield ^{3}**15**$_{AF}$ should occur at a potential of just 0.686 V vs NHE. As this second potential is more negative than the preceding PCET event, this should result in potential inversion associated with a single two-electron event where the observed redox potential is the average of the two single-electron redox potentials.[69−72] For the two proton/two electron coupled transfer event from ^{5}**9** to ^{3}**15**$_{AF}$, this two-electron event is calculated to be observable at 1.000 V vs NHE. However, as the experimental redox events in aqueous solution are irreversible they cannot be directly correlated to our calculated results. Nonetheless, our calculations predict that the formally Mn^{V}-bis(oxo) intermediate ^{3}**15**$_{AF}$ is the most likely candidate to be responsible for O−O bond formation following the electrochemical oxidation.

The electronic structure of intermediate **15** is complicated and we identified six different electronic configurations that are plausible and must be considered. The relative energies of these different electronic arrangements along with diagnostic Mulliken spin densities of the manganese and oxygen atoms, the manganese−oxygen bond lengths, and the oxidation state of the manganese ion with a designation of high spin, intermediate spin, or low spin are given in Table 2.

The ground state, denoted as ^{3}**15**$_{AF}$, exhibits AF coupling between one of the oxygen atoms (O1), which has an excess β-spin density of 0.52, and the Mn-center that has an α-spin population of 2.36. The other oxygen atom O2 has a slightly shorter Mn−O bond length of 1.591 Å compared to 1.620 Å and only a small amount of residual spin density of 0.06, suggesting that this oxygen is appropriately described as a classical oxo moiety. It should be noted that the spin density of 0.52 on O1, while suggestive, does not necessarily indicate an oxyl radical,[33,73] as it is possible that the $Mn^{V}{=}O$ bond is highly covalent in nature and the excess spin density on the oxo fragment is a result of strong π-donation from one of the singly occupied d-π orbitals of the high-spin Mn center. Realistically,

Table 2. Most Plausible Electronic Configurations of 15

	^{5}**15**	^{5}**15**$_{AF}$	^{3}**15**	^{3}**15**$_{AF}$	^{1}**15**	^{1}**15**$_{AF}$
ΔG (kcal mol^{-1})	9.06	12.84	4.28	0.00	28.13	18.37
spin density (Mn)	2.26α	3.49α	1.82α	2.36α	0.30β	0.02β
spin density (O1)	0.90α	1.09α	0.11α	0.52β	0.24α	0.53β
spin density (O2)	0.90α	0.62β	0.15α	0.06α	0.06α	0.55α
Mn−O1 (Å)	1.701	1.818	1.615	1.620	1.587	1.611
Mn−O2 (Å)	1.701	1.696	1.616	1.591	1.580	1.612
Mn ox. state (spin state)[a]	+III (IS)	+III (HS)	+V (HS)	+IV (HS)	+V (LS)	+III (LS)

[a]IS: Intermediate spin state. HS: High-spin state. LS: Low-spin state.

the electronic structure of the $Mn^{V}{=}O$ fragment is best described as a superposition of the two extremes. The oxygens in similar electronic structure patterns have previously been interpreted as being oxyl radicals, as this interpretation provides a convenient rationale for the observed water oxidation reactivity.[34,37,39,63,74−76] An alternative triplet configuration where the metal center has not been reduced by the O1 and retains its +V oxidation state ^{3}**15** is 4.3 kcal mol^{-1} higher in energy than ^{3}**15**$_{AF}$. Two singlet states were found, one of which shows AF coupling between oxyl radicals on each of the oxygen atoms, but these spin configurations are significantly higher in energy by 28.1 and 18.4 kcal mol^{-1} than the triplet ground state and can be safely discarded.

The quintet spin surface also provides two potential spin configurations that both lie higher in energy than ^{3}**15**$_{AF}$, but are low enough to be thermally populated at room temperature. The lowest energy of these configurations ^{5}**15** is 9.1 kcal mol^{-1} above ^{3}**15**$_{AF}$ and has an electronic structure most consistent with an intermediate-spin Mn^{III}. With a Mulliken spin density of 2.26α, the unpaired electrons on the metal are coupled ferromagnetically to the electrons of the oxyl radicals on each of the oxygen atoms. The lengthening of each of the Mn−O bonds to 1.701 Å is consistent with electron transfer from the metal-oxo π-bonding orbital. Located slightly higher in energy at 12.8 kcal mol^{-1} relative to ^{3}**15**$_{AF}$ the other potential quintet configuration ^{5}**15**$_{AF}$ possesses strong AF coupling between the two oxygen atoms having spin densities of 1.09α and 0.62β, respectively. The Mn−O1 bond distance is considerably lengthened to a distance of 1.818 Å compared to the Mn−oxyl bond lengths of 1.701 Å in ^{5}**15**. The exceptionally long bond length along with the particularly high spin density of 1.09α on O1 hints at a significant extent of electron transfer between and O1 and Mn suggesting that some oxene character, that is, oxygen in a formally zero oxidation state, is present. Such a highly oxidized oxygen moiety is expected to be an exceptionally strong oxidant and provide an intuitively understandable explanation for the remarkable oxidative reactivity of the Mn complex. The spin density on Mn of 3.49 is intermediate between high-spin Mn^{III} and intermediate-spin Mn^{II}. The occupations of the metal-based orbitals localized using the Boys localization scheme, however, support the assignment of a high-spin Mn^{III} ion as shown in Figure 3. The high oxidation state of the formally Mn^{V} center results in an inversion of the classical metal-oxo bonding picture, where the Mn−O π orbital is significantly polarized toward the metal and the Mn−O π^* orbital is largely oxo-based.[73,77]

The mechanism generally accepted for O−O bond formation in mononuclear water oxidation catalysts involves nucleophilic

DOI: 10.1021/acs.inorgchem.6b03144
Inorg. Chem. 2017, 56, 4435−4445

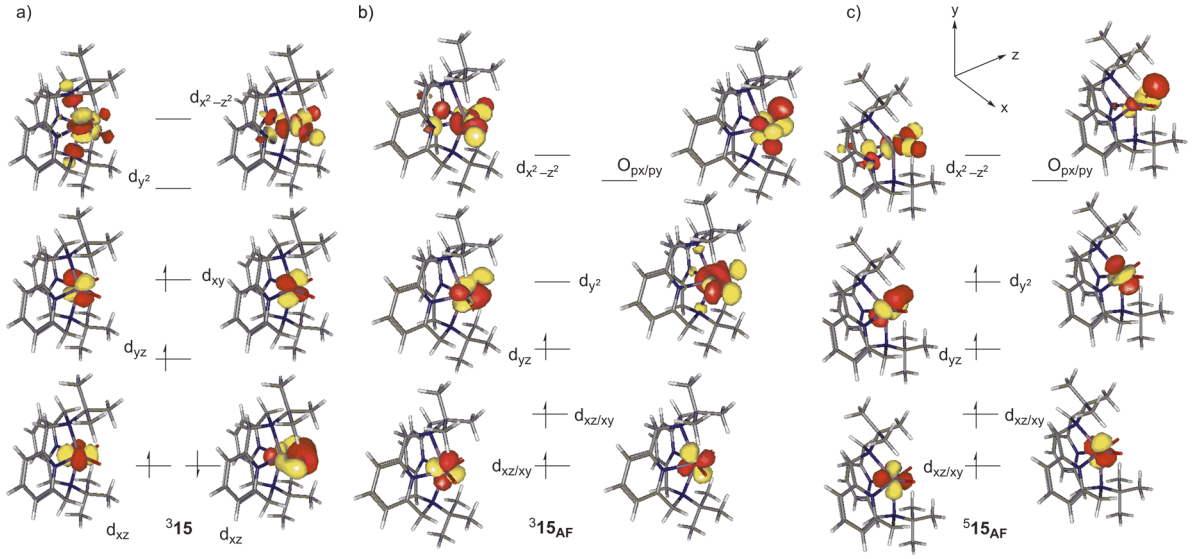

Figure 3. Electronic structures of (a) ^{5}**15**, (b) ^{3}**15**$_{AF}$, and (c) ^{5}**15**$_{AF}$. The unpaired electrons on the oxygen moieties are not shown.

attack of water or hydroxide on a high-valent metal-oxo fragment.[78,79] Radical coupling mechanisms between oxyl radicals on two discrete metal sites have also been proposed,[24,80,81] but the experimentally observed first-order kinetics on catalyst concentration in the current case precludes such a bimolecular pathway. Kusunoki and co-workers have also suggested that two water molecules may couple on a terminal Mn center in a Mn_4Ca cluster.[82] We have extensively sampled the potential energy surface for all plausible spin states and probed several reasonable reaction pathways, illustrated in Figure 4 for the O−O bond formation step.

Despite exhaustive efforts, we were unable to locate any transition state originating directly from the resting state ^{3}**15**$_{AF}$ to afford a reaction barrier that is consistent with a room temperature reaction (vide infra). Interestingly, we found that

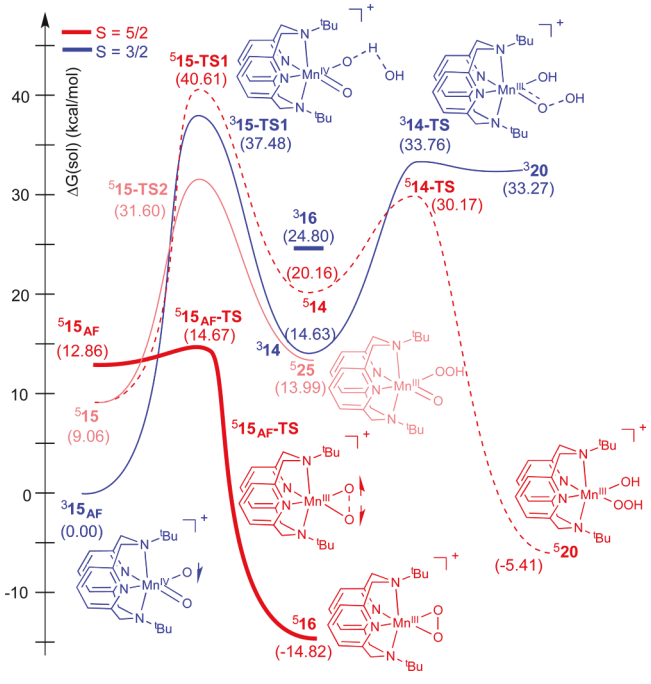

Figure 4. Energy profile for the formation of the O−O bond.

the quintet species ^{5}**15**$_{AF}$ is a much better candidate for promoting the O−O coupling. The transition state that leads to a η^2-bound peroxo intermediate ^{5}**16** is only 1.8 kcal/mol higher than ^{5}**15**$_{AF}$. This reaction trajectory invokes an intersystem crossing (ISC) from the triplet surface where the resting state ^{3}**15**$_{AF}$ is located to the quintet surface to access the low energy transition state ^{5}**15**$_{AF}$**-TS**. The resulting reaction barrier is reasonable at 14.7 kcal/mol, but the intersystem crossing is intrinsically coupled to a significant change in electronic structure in addition to the spin state transition. As highlighted by differing formal oxidation states of the Mn-center in ^{3}**15**$_{AF}$ and ^{5}**15**$_{AF}$, the electronic configurations found in these two complexes cannot be reached by a simple spin flip and requires electron density to be transferred between one of the ligands and the metal center. Formal reduction of the Mn(IV) center in ^{3}**15**$_{AF}$ to Mn(III) in ^{5}**15**$_{AF}$ utilizes one of the lone-pair electrons of the oxo moiety. Following the electron transfer, the two oxyl fragments in ^{5}**15**$_{AF}$ with spin densities of 1.09α and 0.62β, respectively, can combine in a radical coupling reaction to form the peroxo intermediate. The Mulliken spin densities enumerated in Table 2 and the simplified Lewis structures shown in Figure 4 illustrate this process. This is similar to the mechanism proposed by Li et al. of coupling between two oxo fragments on a Mn^V center.[83]

The intersystem crossing from the triplet to the quintet potential energy surface is likely to be challenging to accomplish because of the significant structural change that accompanies the spin crossover, in addition to intrinsic difficulties associated with the spin-forbidden surface hopping process. Both of the equatorial Mn−N bonds contract by about 0.1 Å and the N2−Mn−N3 angle expands from 76° to 84°, whereas both Mn−O bonds lengthen considerably as the Mn−O1 distance increases by 0.198 Å and the Mn−O2 bond elongates by 0.105 Å. The O1−Mn−O2 angle also shrinks considerably from 118° in ^{3}**15**$_{AF}$ to just 90° in ^{5}**15**$_{AF}$. The two oxygen atoms are drawn into a much closer proximity as a result with the O−O distance contracting from 2.756 to 2.485 Å priming the complex for the O−O coupling reaction. The structure of ^{5}**15**$_{AF}$ is very similar to that found at the transition state ^{5}**15**$_{AF}$**-TS** and the resulting product ^{5}**16**, where the only major structural difference is the continued contraction of the

DOI: 10.1021/acs.inorgchem.6b03144
Inorg. Chem. 2017, 56, 4435−4445

O−O distance. Thus, it enables an extremely facile radical coupling reaction between the two oxyl radical fragments of ^{5}**15**$_{AF}$ once it is formed despite the penalty in reaction rate incurred for the intersystem crossing. Radical couplings typically incur no electronic energy penalty, but can become complicated by effects such as solvation for intermolecular radical couplings between ruthenium water oxidation catalysts.[84]

To estimate the energetic cost for reaching the intersystem crossing point on the potential energy surface, we performed a linear synchronous transit scan between the geometries of the reactant structure ^{3}**15**$_{AF}$ and the transition state ^{5}**15**$_{AF}$**-TS**. From the data in Figure 5 it is clear that the triplet state is

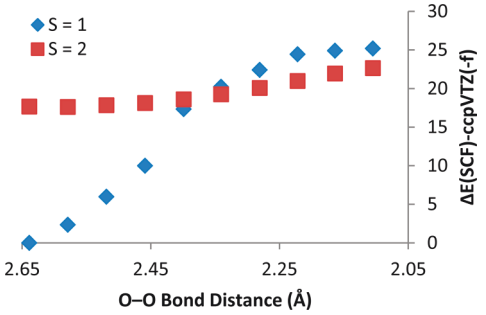

Figure 5. Relative electronic energies of triplet and quintet states in a scan between the geometries of ^{3}**15**$_{AF}$ and ^{5}**15**$_{AF}$**-TS**.

favored on the electronic energy surface until the O−O bond distance contracts to about 2.34 Å. At this point the electronic energy is about 17 kcal mol^{-1} higher than the reactant. However, factors such as entropy and solvation reduce this overall penalty to only 14.7 kcal mol^{-1} at the transition state.

Considering a nucleophilic attack of the Mn−O moiety by water both in a concerted and asynchronous fashion, we were unable to locate a transition state for the concerted addition of water to intermediate **15**. A concerted mechanism is unlikely as each of the otherwise symmetry equivalent oxo fragments would be required to behave differently: one would need to act as a Brønstead base in order to abstract a proton from water, whereas the other oxo moiety would have to function as a Lewis acid toward the incipient hydroxide ion. The calculated barrier to proton transfer to one of the oxo fragments ^{3}**15-TS1** is calculated to be 37.5 kcal mol^{-1} on the triplet surface and 40.6 kcal mol^{-1} through ^{5}**15-TS1** on the quintet surface. Subsequent attack of the resulting hydroxide molecule on the remaining oxo group is indicated by our calculations to be most favorable for the quintet state ^{5}**14-TS** with a barrier of 30.2 kcal mol^{-1}. The transition state for addition of hydroxide on the triplet surface ^{3}**14-TS** was found at 33.8 kcal mol^{-1}. The high barrier to protonation, however, suggests that this pathway is not viable under ambient conditions. Considering that the hydroxyl proton on ^{3}**14** has a calculated pK_a of 1.45, which corresponds to a ΔG(sol) for deprotonation of −14.6 kcal mol^{-1} at pH 12.2, it is not surprising that proton transfer is a prohibitively difficult step. The adduct structures where the hydroxide ion formed after proton transfer to intermediate **15** remains hydrogen bonded to species **14** are less stable than the structures lacking this interaction at 27.5 and 28.2 kcal mol^{-1} higher in energy than ^{3}**15**$_{AF}$ on the triplet and quintet surfaces, respectively. We have also calculated the barrier for directly adding hydroxide to the bis(oxo) intermediate, which occurs on the quintet surface with a barrier of just 15.0 kcal mol^{-1}. However, there is a significant energetic penalty for generating a hydroxide ion from water in aqueous solution, which at pH 12.2 is approximately 16.6 kcal mol^{-1} rendering the overall barrier for the addition of hydroxide via ^{5}**15-TS2** to be 31.6 kcal mol^{-1}.

The presence of two oxygen-based ligands in ^{3}**15**$_{AF}$ in a *cis* arrangement to one another and the fact that the oxyl radicals carry electrons with opposite spin invited the proposition of an intramolecular coupling between radical fragments to generate a Mn^{III}-peroxo intermediate. Despite the weakly coupled AF triplet ^{3}**15**$_{AF}$ being the ground state for the formally Mn^{V}-bis(oxo) intermediate, the intramolecular O−O coupling occurs most favorably on the quintet surface through ^{5}**15**$_{AF}$**-TS** with a barrier of just 14.7 kcal mol^{-1}. This is not surprising as the resulting Mn^{III}-peroxo ^{5}**16** is more stable on the quintet surface by 38.8 kcal mol^{-1} compared to the triplet analogue, ^{3}**16**. The septet ^{7}**16** is the second lowest spin state for the peroxo intermediate and is 13.3 kcal mol^{-1} higher in energy than the quintet. The formation of ^{5}**16** is downhill thermodynamically from ^{3}**15**$_{AF}$ by 14.0 kcal mol^{-1}. This two-state reactivity[85] enabled by the accessible high-spin states provided by the first-row transition metal center facilitates a relatively low barrier for O−O bond formation. The intramolecular coupling on the quintet surface is, of course, facilitated by the AF coupling between the two oxyl radicals exhibited in ^{5}**15**$_{AF}$ rather than the electronic structure in ^{5}**15** featuring parallel α-spins on the oxyl moieties.

This proposed mechanism for O−O bond formation in a mononuclear catalyst is unusual. Intramolecular coupling mechanisms leading to O−O bond formation on mononuclear

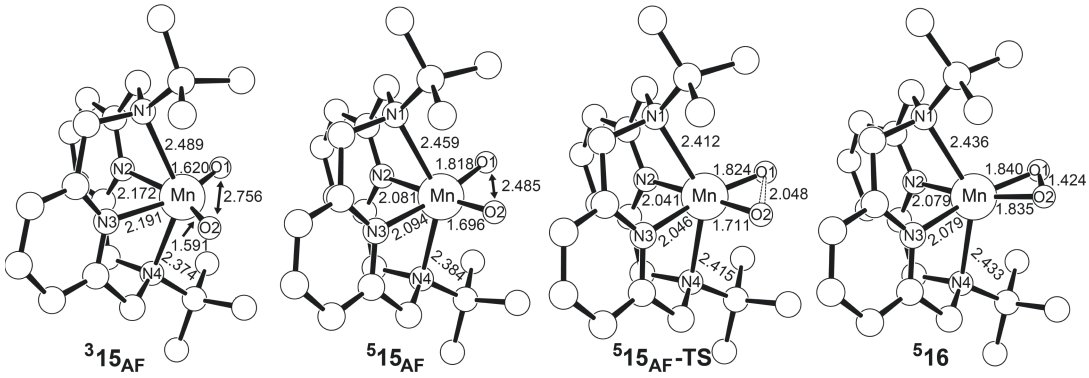

Figure 6. Optimized structures of intermediates during O−O bond formation.

DOI: 10.1021/acs.inorgchem.6b03144
Inorg. Chem. 2017, 56, 4435−4445

catalysts are rare and confined to H_2O_2 generation,[86,87] whereas direct $^3O_2$ production is generally limited to dinuclear catalysts.[88−91] We note that intramolecular O−O bond formation has been proposed during the photodecomposition of MnO_4^-,[92,93] although this reaction only occurs under photochemical conditions.

At the transition state, the structure of which is shown in Figure 6, the Mn−O bond lengths are only increased to 1.824 and 1.711 Å from 1.818 and 1.696 Å in ^{5}**15**$_{AF}$, respectively. The O−O bond distance has decreased significantly to 2.048 Å from 2.464 Å and the O1−Mn−O2 angle decreases from 138.6° to 70.7°. The Mulliken spin density on O1 decreases from 1.01 to 0.93 and increases on O2 from −0.56 to −0.64 along with a decrease on Mn from 3.63 to 3.42.

Li and co-workers ruled out that O−O bond formation should not proceed from a Mn(VI) oxidation state as the potentials required to generate such as state on the metal center are too high in energy.[83] It was not explored, however, as to whether it is even necessary to access the Mn(V) oxidation state the Mn(V) oxidation state to promote water oxidation with to promote water oxidation. Mn(IV) intermediates have been characterized in the OEC.[94] To determine whether it is necessary to access the formal Mn^V oxidation state to facilitate O−O bond formation, or whether the Mn^{IV}-intermediate ^{4}**12** could form the O−O bond, we examined several mechanistic scenarios starting from the $[Mn^{IV}(=O)(OH)]^+$ intermediate ^{4}**12**, as shown in Figure 7. The electronic structure of this species may be best illustrated using the Mulliken spin density on the oxo fragment of −0.706 as $[Mn^{III}(O^{\bullet})(OH)]^+$, where an oxyl radical is AF coupled to a high-spin Mn^{III} ion. Based on our calculated electrochemical potentials we do not expect this species to persist in solution as the calculated potential to access the formally Mn^V-bis(oxo) ^{3}**15** is more negative than the potential to produce ^{4}**12**, which should result in potential inversion where the observed electrochemical event should occur as a single two-electron response.[69−72,95] Nevertheless, to ensure that the ^{4}**12** is not responsible for O−O bond formation we have modeled several different plausible pathways described below.

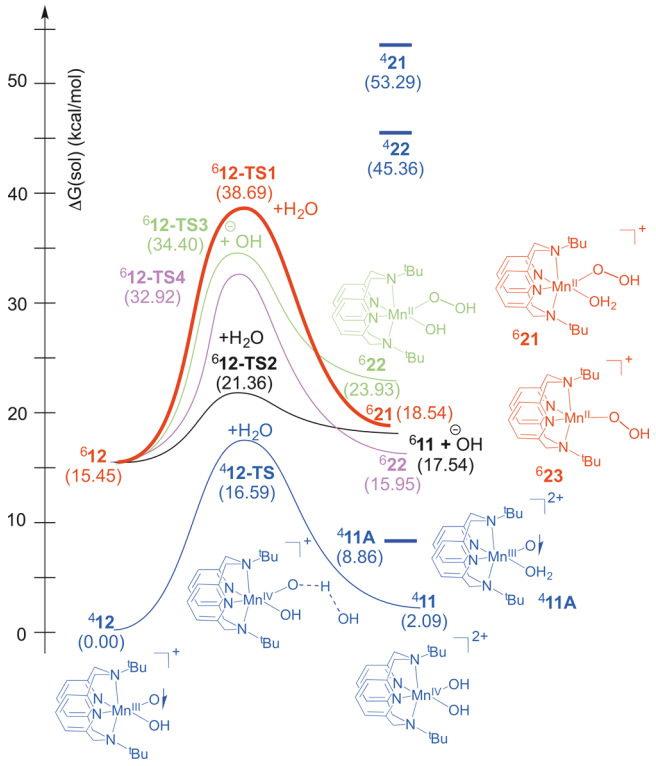

Figure 7. Energetic profile for O−O bond formation at the formal Mn^{IV} oxidation state.

In ^{6}**12** the asymmetry of the oxygen-ligands with one being an oxyl and the other a hydroxyl fragment enables significant radical character on the oxyl fragment. As a result, the transfer of a proton from water to the hydroxyl ligand of ^{6}**12** occurs in a concerted fashion with nucleophilic attack of the incipient hydroxide molecule on the oxyl ligand. The concerted addition of water occurs with a barrier of 38.7 kcal mol^{-1} on the sextet potential energy surface shown in bold red line in Figure 7 producing ^{6}**21**. On the quartet surface, shown in blue in Figure 7, the resulting product ^{4}**21** is 53.3 kcal mol^{-1} higher in energy than the reactant ^{4}**12** making the addition of water not feasible for this spin state. The high energy barrier calculated for this process is not surprising as it requires proton transfer to the less basic hydroxyl fragment relative to the oxo moiety. Transition states for the transfer of a proton from water to the oxyl radical fragment of intermediate **12** were found with barriers of 16.6 and 21.4 kcal mol^{-1} on the quartet and sextet surfaces traversing the transition states ^{4}**12-TS** and ^{6}**12-TS2**, respectively. The hydroxyl protons on the water addition product ^{4}**11** have a calculated pK_a of 10.7, which suggests that this intermediate should readily deprotonate under experimental conditions. Moreover, the bis(hydroxyl) intermediate is not expected to be active for O−O bond formation. Protonation of the hydroxyl ligand of ^{4}**12** rather than the more basic oxo fragment in ^{4}**11A** is thermodynamically uphill by 8.9 kcal mol^{-1} and the expected kinetic barrier to proton transfer should also be more difficult to overcome. Attempts to find the transition states for the asynchronous proton transfer to the hydroxyl ligand instead were unsuccessful. The barrier for the subsequent addition of hydroxide is expected to be more difficult for ^{4}**11A** compared to ^{3}**14** as the less oxidizing Mn^{III} center of ^{4}**11A** will not render the bound oxo moiety as nucleophilic as the Mn^{IV} center of ^{3}**14**. Therefore, even if proton transfer is possible to ^{4}**11A**, the following addition of hydroxide should be more difficult than the 30.2 kcal mol^{-1} calculated for ^{5}**14-TS**.

The direct addition of hydroxide to intermediate ^{4}**12** results in an intermediate ^{4}**22** that is 45.4 kcal mol^{-1} above ^{4}**12**. Such hydroxide addition is more favorable on the sextet surface through ^{6}**12-TS3**, depicted in green in Figure 7, with a barrier of 34.4 kcal mol^{-1}, but this is still too high to be viable under ambient conditions. An intramolecular coupling, shown in magenta color in Figure 7, between the hydroxyl fragment and the oxo group furnishing ^{6}**23** was explored and is also more favorable on the sextet surface with a barrier via ^{6}**12-TS4** of 32.9 kcal mol^{-1}, which is again not a meaningful reaction trajectory under experimental conditions. All these calculations suggest that oxidation of water is not possible at the Mn^{IV} oxidation state and that further oxidation to Mn^V is necessary.

The complete mechanism for catalytic water oxidation is summarized in Figure 8. The aforementioned discussion covered the most difficult and complicated portion up to the formation of the Mn^{III}-peroxo intermediate ^{5}**16**. To complete the catalytic cycle, one additional electron must be removed. Addition of a water molecule to ^{5}**16** prior to oxidation is uphill by 5.9 kcal mol^{-1}. The oxidation occurs with a calculated potential of 1.169 V vs NHE and the electron is removed from

DOI: 10.1021/acs.inorgchem.6b03144
Inorg. Chem. 2017, 56, 4435−4445

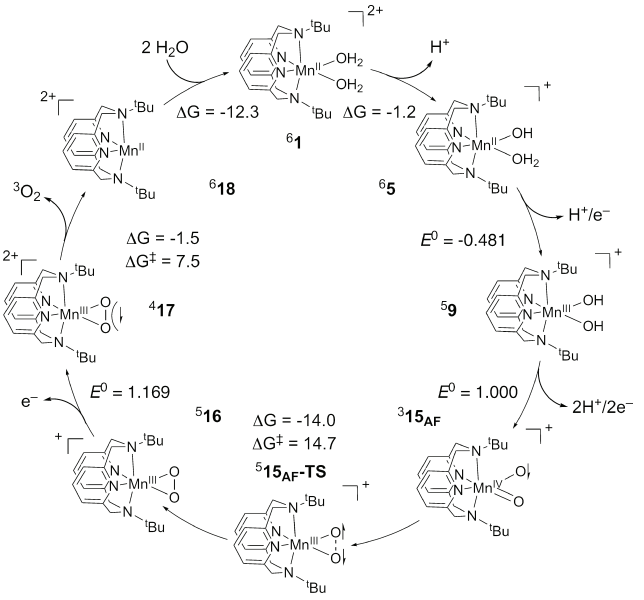

Figure 8. Proposed catalytic cycle for water oxidation.

the peroxo ligand in ^{4}**17** rather than the Mn as the spin density on Mn increases from 4.111 to 4.223. The calculated potential of 1.169 V is close to the approximate onset potential for catalysis at ∼1.3 V. The amount of β-spin density increases from −0.101 and −0.097 to −0.672 and −0.693 on each of the oxygen atoms, respectively. The sextet ^{6}**17**, where the superoxyl fragment is ferromagnetically coupled to the Mn-center, is 6.2 kcal mol^{-1} higher in energy than the energetically more favorable antiferromagnetically coupled alternative ^{4}**17**. Intramolecular transfer of an electron from the superoxyl moiety in ^{4}**17** to Mn produces a HS Mn^{II} ion AF coupled to triplet dioxygen. Release of $^3O_2$ takes place with a calculated barrier of 7.5 kcal mol^{-1} and is energetically favorable by 1.5 kcal mol^{-1}. Complexation of two molecules of water to the resulting four coordinate intermediate ^{5}**18** regenerates ^{6}**1** and is downhill by 12.3 kcal mol^{-1} to complete the catalytic cycle.

CONCLUSIONS

In summary, our calculations have demonstrated that the oxidation of water by $[Mn(Py_2N^tBu_2)(H_2O)_2]^{2+}$ should proceed through a Mn^V-bis(oxo) intermediate that is accessed by a series of proton-coupled electron transfer events. The second of these redox events is calculated to be the concerted removal of two electrons along with two protons with inverted ordering of the redox potentials. That is, the second PCET is more favorable than the first. The ground state of the Mn^V-bis(oxo) species is the triplet state, but our calculations suggest that a thermally accessible quintet state displaying AF coupling between two oxyl radical fragments facilitates O−O bond formation with a calculated barrier of just 14.7 kcal mol^{-1}. Through the understanding gained by elucidating the electronic structure of the catalytically competent intermediate is possible to understand how two terminal aqua ligands may be coupled to form a peroxide intermediate. Further oxidation of the resulting Mn^{III}-peroxo species gives a Mn^{III}-superoxyl intermediate that can transfer an electron from the superoxyl moiety to Mn to release triplet dioxygen and regenerate the initial Mn^{II} state. This work furthers our understanding of how the accessible high-spin states available for first-row transition metal ions enhance the oxidative reactivity of homogeneous water oxidation catalysts.

Our results also provide insight into the critical role played by the pyridinophane ligand in facilitating catalytic water oxidation. In addition to providing the appropriate electronic environment for accessing multiple oxidation and spin states, the geometry and flexibility of this ligand is critical to O−O bond formation. Specifically, in addition to creating the *cis*-divacant octahedral environment required for the intramolecular O−O bond coupling event, the flexibility of the ligand in traversing a range of N2−Mn−N3 bond angles promotes efficient O−O coupling with a low energy barrier of only ∼15 kcal mol^{-1}. Our computer model identifies the key challenge to overcome to be the intersystem crossing from the triplet to the quintet states, which may lower the rate of the reaction significantly despite the low energy transition state. Whereas a detailed examination of the spin−orbit coupling and the surface hopping mechanism was beyond the scope of this study, it is safe to assume that the relatively low effective nuclear charge of the first row transition metal manganese gives rise to an insufficiently strong spin−orbit coupling. Future work must therefore address how to increase the intersystem crossing rate and whereas further lowering the already low transition state energy of ∼15 kcal mol^{-1} may be possible, increasing the spin−orbit coupling to facilitate the spin-forbidden transition state is a more promising strategy.

Finally, we note that our proposed O−O coupling mechanism shares similarities with O−O bond formation proposals that involve the coupling of two terminal aqua ligands in Photosystem II,[14] but the details revealed here are entirely different. While the currently favored mechanism for O_2 evolution involves bond formation in the center of the OEC between an oxyl radical and a bridging oxo ligand, an alternative proposal involves the coupling of two terminal water molecules bound to the dangling manganese ion of the tetramanganese cluster.[96] Such a pathway can avoid the potentially high energy barrier to O−O formation using a bridging oxo.[12,14,38,97,98] In this case, the single Mn ion must access a + V oxidation state, whereas the multiple metal centers of the enables the reaction in the OEC using lower oxidation states. Importantly, our mechanism shows that intramolecular O−O coupling at a single manganese ion is thermally accessible, and it can occur with a barrier that is similar to that observed for Photosystem II. As anticipated anecdotally among mechanistic researchers, the spin states and intersystem crossings of the high-valent manganese complex play a critical role and our study provides a detailed map of such mechanism. Studies that attempt to confirm our proposed mechanism experimentally and exploit the mechanistic insight into designing improved catalysts are currently underway in our laboratories.

ASSOCIATED CONTENT

Supporting Information

The Supporting Information is available free of charge on the ACS Publications website at DOI: 10.1021/acs.inorgchem.6b03144.

Listings of Cartesian coordinates of all structures, energies, and computed redox potentials, and additional discussion (PDF)

DOI: 10.1021/acs.inorgchem.6b03144
Inorg. Chem. 2017, 56, 4435−4445

AUTHOR INFORMATION

Corresponding Authors

*E-mail: smith962@indiana.edu.
*E-mail: mbaik2805@kaist.ac.kr.

ORCID

Jeremy M. Smith: 0000-0002-3206-4725
Mu-Hyun Baik: 0000-0002-8832-8187

Notes

The authors declare no competing financial interest.

ACKNOWLEDGMENTS

We thank the Institute for Basic Science (IBS-R10-D1) in Korea, the ACS-PRF (50971-ND3 to J.M.S.), the National Science Foundation (CHE-1566258 to J.M.S.), and the Research Corporation (Scialog Award to M.H.B.) for support.

REFERENCES

(1) Lewis, N. S.; Nocera, D. G. Powering the planet: chemical challenges in solar energy utilization. *Proc. Natl. Acad. Sci. U. S. A.* **2006**, *103*, 15729−15735.

(2) Lewis, N. S.; Nocera, D. G. Powering the planet: chemical challenges in solar energy utilization. [Erratum to document cited in CA146:103702]. *Proc. Natl. Acad. Sci. U. S. A.* **2007**, *104*, 20142.

(3) Alstrum-Acevedo, J. H.; Brennaman, M. K.; Meyer, T. J. Chemical Approaches to Artificial Photosynthesis. 2. *Inorg. Chem.* **2005**, *44*, 6802−6827.

(4) Gust, D.; Moore, T. A.; Moore, A. L. Mimicking Photosynthetic Solar Energy Transduction. *Acc. Chem. Res.* **2001**, *34*, 40−48.

(5) Gilbert, J. A.; Eggleston, D. S.; Murphy, W. R.; Geselowitz, D. A.; Gersten, S. W.; Hodgson, D. J.; Meyer, T. J. Structure and Redox Properties of the Water-Oxidation Catalyst (bpy)2(OH2)RuORu-(OH2) (bpy)2 4+. *J. Am. Chem. Soc.* **1985**, *107*, 3855−3864.

(6) Liu, X.; Wang, F. Transition metal complexes that catalyze oxygen formation from water: 1979−2010. *Coord. Chem. Rev.* **2012**, *256*, 1115−1136.

(7) Umena, Y.; Kawakami, K.; Shen, J.-R.; Kamiya, N. Crystal structure of oxygen-evolving photosystem II at a resolution of 1.9[thinsp]A. *Nature* **2011**, *473*, 55−60.

(8) McEvoy, J. P.; Brudvig, G. W. Water-Splitting Chemistry of Photosystem II. *Chem. Rev.* **2006**, *106*, 4455−4483.

(9) Wu, A. J.; Penner-Hahn, J. E.; Pecoraro, V. L. Structural, Spectroscopic, and Reactivity Models for the Manganese Catalases. *Chem. Rev.* **2004**, *104*, 903−938.

(10) Antonyuk, S. V.; Melik-Adamyan, V. R.; Popov, A. N.; Lamzin, V. S.; Hempstead, P. D.; Harrison, P. M.; Artymyuk, P. J.; Barynin, V. V. Three-dimensional structure of the enzyme dimanganese catalase from Thermus Thermophilus at 1 Å resolution. *Crystallogr. Rep.* **2000**, *45*, 105−116.

(11) Barynin, V. V.; Whittaker, M. M.; Antonyuk, S. V.; Lamzin, V. S.; Harrison, P. M.; Artymiuk, P. J.; Whittaker, J. W. Crystal Structure of Manganese Catalase from Lactobacillus plantarum. *Structure* **2001**, *9*, 725−738.

(12) Siegbahn, P. E. M. Structures and Energetics for O2 Formation in Photosystem II. *Acc. Chem. Res.* **2009**, *42*, 1871−1880.

(13) Yamanaka, S.; Isobe, H.; Kanda, K.; Saito, T.; Umena, Y.; Kawakami, K.; Shen, J. R.; Kamiya, N.; Okumura, M.; Nakamura, H.; Yamaguchi, K. Possible mechanisms for the O−O bond formation in oxygen evolution reaction at the CaMn4O5(H2O)4 cluster of PSII refined to 1.9 Å X-ray resolution. *Chem. Phys. Lett.* **2011**, *511*, 138−145.

(14) Shen, J.-R. The Structure of Photosystem II and the Mechanism of Water Oxidation in Photosynthesis. *Annu. Rev. Plant Biol.* **2015**, *66*, 23−48.

(15) Artero, V.; Fontecave, M. Solar fuels generation and molecular systems: is it homogeneous or heterogeneous catalysis? *Chem. Soc. Rev.* **2013**, *42*, 2338−2356.

(16) Shimazaki, Y.; Nagano, T.; Takesue, H.; Ye, B.-H.; Tani, F.; Naruta, Y. Characterization of a Dinuclear MnV?O Complex and Its Efficient Evolution of O2 in the Presence of Water. *Angew. Chem., Int. Ed.* **2004**, *43*, 98−100.

(17) Gao, Y.; Åkermark, T.; Liu, J.; Sun, L.; Åkermark, B. Nucleophilic Attack of Hydroxide on a MnV Oxo Complex: A Model of the O−O Bond Formation in the Oxygen Evolving Complex of Photosystem II. *J. Am. Chem. Soc.* **2009**, *131*, 8726−8727.

(18) Cady, C. W.; Crabtree, R. H.; Brudvig, G. W. Functional models for the oxygen-evolving complex of photosystem II. *Coord. Chem. Rev.* **2008**, *252*, 444−455.

(19) Wiechen, M.; Berends, H.-M.; Kurz, P. Water oxidation catalysed by manganese compounds: from complexes to 'biomimetic rocks'. *Dalton Transactions* **2012**, *41*, 21−31.

(20) Karlsson, E. A.; Lee, B.-L.; Åkermark, T.; Johnston, E. V.; Kärkäs, M. D.; Sun, J.; Hansson, Ö.; Bäckvall, J.-E.; Åkermark, B. Photosensitized Water Oxidation by Use of a Bioinspired Manganese Catalyst. *Angew. Chem., Int. Ed.* **2011**, *50*, 11715−11718.

(21) Gao, Y.; Crabtree, R. H.; Brudvig, G. W. Water Oxidation Catalyzed by the Tetranuclear Mn Complex [MnIV4O5(terpy)4-(H2O)2](ClO4)6. *Inorg. Chem.* **2012**, *51*, 4043−4050.

(22) Seidler-Egdal, R. K.; Nielsen, A.; Bond, A. D.; Bjerrum, M. J.; McKenzie, C. J. High turnover catalysis of water oxidation by Mn(ii) complexes of monoanionic pentadentate ligands. *Dalton Transactions* **2011**, *40*, 3849−3858.

(23) Young, K. J.; Takase, M. K.; Brudvig, G. W. An Anionic N-Donor Ligand Promotes Manganese-Catalyzed Water Oxidation. *Inorg. Chem.* **2013**, *52*, 7615−7622.

(24) Yoshida, M.; Masaoka, S.; Abe, J.; Sakai, K. Catalysis of Mononuclear Aquaruthenium Complexes in Oxygen Evolution from Water: A New Radical Coupling Path using Hydroxocerium(IV) Species. *Chem. - Asian J.* **2010**, *5*, 2369−2378.

(25) Chen, H.; Tagore, R.; Olack, G.; Vrettos, J. S.; Weng, T.-C.; Penner-Hahn, J.; Crabtree, R. H.; Brudvig, G. W. Speciation of the Catalytic Oxygen Evolution System: [MnIII/IV2(μ-O)2(terpy)2-(H2O)2](NO3)3 + HSO5. *Inorg. Chem.* **2007**, *46*, 34−43.

(26) Wasylenko, D. J.; Ganesamoorthy, C.; Henderson, M. A.; Koivisto, B. D.; Osthoff, H. D.; Berlinguette, C. P. Electronic Modification of the [RuII(tpy) (bpy) (OH2)]2+ Scaffold: Effects on Catalytic Water Oxidation. *J. Am. Chem. Soc.* **2010**, *132*, 16094−16106.

(27) Wasylenko, D. J.; Ganesamoorthy, C.; Henderson, M. A.; Berlinguette, C. P. Unraveling the Roles of the Acid Medium, Experimental Probes, and Terminal Oxidant, (NH4)2[Ce(NO3)6], in the Study of a Homogeneous Water Oxidation Catalyst. *Inorg. Chem.* **2011**, *50*, 3662−3672.

(28) Parent, A. R.; Crabtree, R. H.; Brudvig, G. W. Comparison of primary oxidants for water-oxidation catalysis. *Chem. Soc. Rev.* **2013**, *42*, 2247−2252.

(29) Hetterscheid, D. G. H.; Reek, J. N. H. Periodate as an Oxidant for Catalytic Water Oxidation: Oxidation via Electron Transfer or O-Atom Transfer? *Eur. J. Inorg. Chem.* **2014**, *2014*, 742−749.

(30) Gao, Y.; Liu, J.; Wang, M.; Na, Y.; Åkermark, B.; Sun, L. Synthesis and characterization of manganese and copper corrole xanthene complexes as catalysts for water oxidation. *Tetrahedron* **2007**, *63*, 1987−1994.

(31) Naruta, Y.; Sasayama, M.; Sasaki, T. Oxygen Evolution by Oxidation of Water with Manganese Porphyrin Dimers. *Angew. Chem., Int. Ed. Engl.* **1994**, *33*, 1839−1841.

(32) Lee, W.-T.; Muñoz, S. B.; Dickie, D. A.; Smith, J. M. Ligand Modification Transforms a Catalase Mimic into a Water Oxidation Catalyst. *Angew. Chem., Int. Ed.* **2014**, *53*, 9856−9859.

(33) Lassalle-Kaiser, B.; Hureau, C.; Pantazis, D. A.; Pushkar, Y.; Guillot, R.; Yachandra, V. K.; Yano, J.; Neese, F.; Anxolabehere-Mallart, E. Activation of a water molecule using a mononuclear Mn complex: from Mn-aquo, to Mn-hydroxo, to Mn-oxyl via charge compensation. *Energy Environ. Sci.* **2010**, *3*, 924−938.

(34) Siegbahn, P. E. M. O···O Bond Formation in the S4 State of the Oxygen-Evolving Complex in Photosystem II. *Chem. - Eur. J.* **2006**, *12*, 9217−9227.

DOI: 10.1021/acs.inorgchem.6b03144
Inorg. Chem. 2017, 56, 4435−4445

(35) Messinger, J. Evaluation of different mechanistic proposals for water oxidation in photosynthesis on the basis of Mn4OxCa structures for the catalytic site and spectroscopic data. *Phys. Chem. Chem. Phys.* **2004**, *6*, 4764−4771.
(36) Liang, W.; Roelofs, T. A.; Cinco, R. M.; Rompel, A.; Latimer, M. J.; Yu, W. O.; Sauer, K.; Klein, M. P.; Yachandra, V. K. Structural Change of the Mn Cluster during the S2→S3 State Transition of the Oxygen-Evolving Complex of Photosystem II. Does It Reflect the Onset of Water/Substrate Oxidation? Determination by Mn X-ray Absorption Spectroscopy. *J. Am. Chem. Soc.* **2000**, *122*, 3399−3412.
(37) Siegbahn, P. E. M. Theoretical Models for the Oxygen Radical Mechanism of Water Oxidation and of the Water Oxidizing Complex of Photosystem II. *Inorg. Chem.* **2000**, *39*, 2923−2935.
(38) Siegbahn, P. E. M. A Structure-Consistent Mechanism for Dioxygen Formation in Photosystem II. *Chem. - Eur. J.* **2008**, *14*, 8290−8302.
(39) Yang, X.; Baik, M.-H. Electronic Structure of the Water-Oxidation Catalyst [(bpy)2(OHx)RuORu(OHy) (bpy)2]z+: Weak Coupling between the Metal Centers Is Preferred over Strong Coupling. *J. Am. Chem. Soc.* **2004**, *126*, 13222−13223.
(40) Crandell, D. W.; Ghosh, S.; Berlinguette, C. P.; Baik, M.-H. How a [CoIV$\hat{}${{\underline{.....}}}$O]2+ Fragment Oxidizes Water: Involvement of a Biradicaloid [CoII−(O$^{\bullet}$)]2+ Species in Forming the O$^{\bullet}$ O Bond. *ChemSusChem* **2015**, *8*, 844−852.
(41) Parr, R. G.; Yang, W. *Density Functional Theory of Atoms and Molecules*; Oxford University Press: New York, 1989.
(42) Ziegler, T. Approximate Density Functional Theory as a Practical Tool in Molecular Energetics and Dynamics. *Chem. Rev.* **1991**, *91*, 651−667.
(43) *Jaguar*, version 8.1; Schrödinger, Inc.: New York, 2014.
(44) Zhao, Y.; Truhlar, D. The M06 suite of density functionals for main group thermochemistry, thermochemical kinetics, noncovalent interactions, excited states, and transition elements: two new functionals and systematic testing of four M06-class functionals and 12 other functionals. *Theor. Chem. Acc.* **2008**, *120*, 215−241.
(45) Slater, J. C. *Quantum Theory of Molecules and Solids, Vol. 4: The Self-Consistent Field for Molecules and Solids*; McGraw-Hill: New York, 1974.
(46) Vosko, S. H.; Wilk, L.; Nusair, M. Accurate Spin-Dependent Electron Liquid Correlation Energies for Local Spin-Density Calculations - a Critical Analysis. *Can. J. Phys.* **1980**, *58*, 1200−1211.
(47) Petersson, G. A.; Bennett, A.; Tensfeldt, T. G.; Al-Laham, M. A.; Shirley, W. A.; Mantzaris, J. A complete basis set model chemistry. I. The total energies of closed-shell atoms and hydrides of the first-row elements. *J. Chem. Phys.* **1988**, *89*, 2193−2218.
(48) Petersson, G. A.; Al-Laham, M. A. A complete basis set model chemistry. II. Open-shell systems and the total energies of the first-row atoms. *J. Chem. Phys.* **1991**, *94*, 6081−6090.
(49) Hay, P. J.; Wadt, W. R. Ab initio Effective Core Potentials for Molecular Calculations - Potentials for the Transition-Metal Atoms Sc to Hg. *J. Chem. Phys.* **1985**, *82*, 270−283.
(50) Wadt, W. R.; Hay, P. J. Ab initio Effective Core Potentials for Molecular Calculations - Potentials for Main Group Elements Na to Bi. *J. Chem. Phys.* **1985**, *82*, 284−298.
(51) Hay, P. J.; Wadt, W. R. Ab initio Effective Core Potentials for Molecular Calculations - Potentials for K to Au Including the Outermost Core Orbitals. *J. Chem. Phys.* **1985**, *82*, 299−310.
(52) Dunning, T. H., Jr. Gaussian basis sets for use in correlated molecular calculations. I. The atoms boron through neon and hydrogen. *J. Chem. Phys.* **1989**, *90*, 1007−1023.
(53) Marten, B.; Kim, K.; Cortis, C.; Friesner, R. A.; Murphy, R. B.; Ringnalda, M. N.; Sitkoff, D.; Honig, B. New Model for Calculation of Solvation Free Energies: Correction of Self-Consistent Reaction Field Continuum Dielectric Theory for Short-Range Hydrogen-Bonding Effects. *J. Phys. Chem.* **1996**, *100*, 11775−11788.
(54) Friedrichs, M.; Zhou, R. H.; Edinger, S. R.; Friesner, R. A. Poisson-Boltzmann Analytical Gradients for Molecular Modeling Calculations. *J. Phys. Chem. B* **1999**, *103*, 3057−3061.
(55) Edinger, S. R.; Cortis, C.; Shenkin, P. S.; Friesner, R. A. Solvation Free Energies of Peptides: Comparison of Approximate Continuum Solvation Models With Accurate Solution of the Poisson-Boltzmann Equation. *J. Phys. Chem. B* **1997**, *101*, 1190−1197.
(56) Rashin, A. A.; Honig, B. Reevaluation of the Born Model of Ion Hydration. *J. Phys. Chem.* **1985**, *89*, 5588−5593.
(57) Noodleman, L.; Lovell, T.; Han, W.-G.; Li, J.; Himo, F. Quantum Chemical Studies of Intermediates and Reaction Pathways in Selected Enzymes and Catalytic Synthetic Systems. *Chem. Rev. (Washington, DC, U. S.)* **2004**, *104*, 459−508.
(58) Noodleman, L. Valence Bond Description of Anti-Ferromagnetic Coupling in Transition-Metal Dimers. *J. Chem. Phys.* **1981**, *74*, 5737−5743.
(59) Noodleman, L.; Davidson, E. R. Ligand spin polarization and antiferromagnetic coupling in transition metal dimers. *Chem. Phys.* **1986**, *109*, 131−143.
(60) Tissandier, M. D.; Cowen, K. A.; Feng, W. Y.; Gundlach, E.; Cohen, M. H.; Earhart, A. D.; Coe, J. V.; Tuttle, T. R., Jr. The Proton's Absolute Aqueous Enthalpy and Gibbs Free Energy of Solvation from Cluster-Ion Solvation Data. *J. Phys. Chem. A* **1998**, *102*, 7787−7794.
(61) Kelly, C. P.; Cramer, C. J.; Truhlar, D. G. Aqueous Solvation Free Energies of Ions and Ion-Water Clusters Based on an Accurate Value for the Absolute Aqueous Solvation Free Energy of the Proton. *J. Phys. Chem. B* **2006**, *110*, 16066−16081.
(62) Minenkov, Y.; Singstad, A.; Occhipinti, G.; Jensen, V. R. The accuracy of DFT-optimized geometries of functional transition metal compounds: a validation study of catalysts for olefin metathesis and other reactions in the homogeneous phase. *Dalton Transactions* **2012**, *41*, 5526−5541.
(63) Siegbahn, P. E. M.; Crabtree, R. H. Manganese Oxyl Radical Intermediates and O−O Bond Formation in Photosynthetic Oxygen Evolution and a Proposed Role for the Calcium Cofactor in Photosystem II. *J. Am. Chem. Soc.* **1999**, *121*, 117−127.
(64) Messinger, J.; Badger, M.; Wydrzynski, T. Detection of one slowly exchanging substrate water molecule in the S3 state of photosystem II. *Proc. Natl. Acad. Sci. U. S. A.* **1995**, *92*, 3209−3213.
(65) Baik, M.-H.; Friesner, R. A. Computing Redox Potentials in Solution: Density Functional Theory as A Tool for Rational Design of Redox Agents. *J. Phys. Chem. A* **2002**, *106*, 7407−7412.
(66) Hammes-Schiffer, S.; Iordanova, N. Theoretical studies of proton-coupled electron transfer reactions. *Biochim. Biophys. Acta, Bioenerg.* **2004**, *1655*, 29−36.
(67) Solis, B. H.; Hammes-Schiffer, S. Proton-Coupled Electron Transfer in Molecular Electrocatalysis: Theoretical Methods and Design Principles. *Inorg. Chem.* **2014**, *53*, 6427−6443.
(68) McCormick, M. C.; Keijzer, K.; Polavarapu, A.; Schultz, F. A.; Baik, M.-H. Understanding Intrinsically Irreversible, Non-Nernstian, Two-Electron Redox Processes: A Combined Experimental and Computational Study of the Electrochemical Activation of Platinum-(IV) Antitumor Prodrugs. *J. Am. Chem. Soc.* **2014**, *136*, 8992−9000.
(69) Lord, R. L.; Schauer, C. K.; Schultz, F. A.; Baik, M.-H. Ring-Slippage and Multielectron Redox Properties of Fe/Ru/Os-Bis(arene) Complexes: Does Hapticity Change Really Cause Potential Inversion? *J. Am. Chem. Soc.* **2011**, *133*, 18234−18242.
(70) Evans, D. H. One-electron and two-electron transfers in electrochemistry and homogeneous solution reactions. *Chem. Rev.* **2008**, *108*, 2113−2144.
(71) Evans, D. H.; Hu, K. Inverted potentials in two-electron processes in organic electrochemistry. *J. Chem. Soc., Faraday Trans.* **1996**, *92*, 3983−3990.
(72) Evans, D. H.; et al. The Kinetic Burden of Potential Inversion in Two-Electron Electrochemical Reactions. *Acta Chem. Scand.* **1998**, *52*, 194−197.
(73) Sameera, W. M. C.; McGrady, J. E. The role of substrate in unmasking oxyl character in oxomanganese complexes: the key to selectivity? *Dalton Transactions* **2008**, 6141−6149.
(74) Lundberg, M.; Blomberg, M. R. A.; Siegbahn, P. E. M. Oxyl Radical Required for O−O Bond Formation in Synthetic Mn-Catalyst. *Inorg. Chem.* **2004**, *43*, 264−274.

DOI: 10.1021/acs.inorgchem.6b03144
Inorg. Chem. 2017, 56, 4435−4445

(75) Yang, X.; Baik, M.-H. Cis,cis-[(bpy)2RuVO]2O4+ Catalyzes Water Oxidation formally via in situ Generation of radicaloid RuIV-O(dot). *J. Am. Chem. Soc.* **2006**, *128*, 7476−7485.
(76) Lundberg, M.; Siegbahn, P. E. M. Theoretical investigations of structure and mechanism of the oxygen-evolving complex in PSII. *Phys. Chem. Chem. Phys.* **2004**, *6*, 4772−4780.
(77) Gebhard, M. S.; Koch, S. A.; Millar, M.; Devlin, F. J.; Stephens, P. J.; Solomon, E. I. Single-crystal spectroscopic studies of Fe(SR)42-(R = 2-(Ph)C6H4): electronic structure of the ferrous site in rubredoxin. *J. Am. Chem. Soc.* **1991**, *113*, 1640−1649.
(78) Betley, T. A.; Wu, Q.; Van Voorhis, T.; Nocera, D. G. Electronic Design Criteria for O−O Bond Formation via Metal−Oxo Complexes. *Inorg. Chem.* **2008**, *47*, 1849−1861.
(79) Cao, R.; Lai, W.; Du, P. Catalytic water oxidation at single metal sites. *Energy Environ. Sci.* **2012**, *5*, 8134−8157.
(80) Nyhlén, J.; Duan, L.; Åkermark, B.; Sun, L.; Privalov, T. Evolution of O2 in a Seven-Coordinate RuIV Dimer Complex with a [HOHOH]− Bridge: A Computational Study. *Angew. Chem., Int. Ed.* **2010**, *49*, 1773−1777.
(81) Duan, L.; Bozoglian, F.; Mandal, S.; Stewart, B.; Privalov, T.; Llobet, A.; Sun, L. A molecular ruthenium catalyst with water-oxidation activity comparable to that of photosystem II. *Nat. Chem.* **2012**, *4*, 418−423.
(82) Kusunoki, M. Mono-manganese mechanism of the photosytem II water splitting reaction by a unique Mn4Ca cluster. *Biochim. Biophys. Acta, Bioenerg.* **2007**, *1767*, 484−492.
(83) Li, Y.; Ye, K.; Siegbahn, P. E. M.; Liao, R.-Z. Mechanism of Water Oxidation Catalysed by a Mononuclear Manganese Complex $[Py_2N(tBu)_2Mn(H_2O)_2]^{2+}$. *ChemSusChem* **2017**, *10*, 903.
(84) Fan, T.; Zhan, S.; Ahlquist, M. S. G. Why Is There a Barrier in the Coupling of Two Radicals in the Water Oxidation Reaction? *ACS Catal.* **2016**, *6*, 8308−8312.
(85) Schröder, D.; Shaik, S.; Schwarz, H. Two-State Reactivity as a New Concept in Organometallic Chemistry§. *Acc. Chem. Res.* **2000**, *33*, 139−145.
(86) Kohl, S. W.; Weiner, L.; Schwartsburd, L.; Konstantinovski, L.; Shimon, L. J. W.; Ben-David, Y.; Iron, M. A.; Milstein, D. Consecutive Thermal H2 and Light-Induced O2 Evolution from Water Promoted by a Metal Complex. *Science* **2009**, *324*, 74−77.
(87) Yang, X.; Hall, M. B. Mechanism of Water Splitting and Oxygen−Oxygen Bond Formation by a Mononuclear Ruthenium Complex. *J. Am. Chem. Soc.* **2010**, *132*, 120−130.
(88) Yang, X.; Baik, M.-H. The Mechanism of Water Oxidation Catalysis Promoted by tPyRU(IV)═O (2)L(3+): A Computational Study. *J. Am. Chem. Soc.* **2008**, *130*, 16231−16240.
(89) Ghosh, S.; Baik, M.-H. The Mechanism of O• O Bond Formation in Tanaka's Water Oxidation Catalyst. *Angew. Chem., Int. Ed.* **2012**, *51*, 1221−1224.
(90) Bozoglian, F.; Romain, S.; Ertem, M. Z.; Todorova, T. K.; Sens, C.; Mola, J.; Rodríguez, M.; Romero, I.; Benet-Buchholz, J.; Fontrodona, X.; Cramer, C. J.; Gagliardi, L.; Llobet, A. The Ru−Hbpp Water Oxidation Catalyst. *J. Am. Chem. Soc.* **2009**, *131*, 15176−15187.
(91) Wada, T.; Ohtsu, H.; Tanaka, K. Catalytic Four-Electron Oxidation of Water by Intramolecular Coupling of the Oxo Ligands of a Bis(ruthenium−bipyridine) Complex. *Chem. - Eur. J.* **2012**, *18*, 2374−2381.
(92) Lee, D. G.; Moylan, C. R.; Hayashi, T.; Brauman, J. I. Photochemistry of aqueous permanganate ion. *J. Am. Chem. Soc.* **1987**, *109*, 3003−3010.
(93) Thornley, W. A.; Bitterwolf, T. E. Photochemistry of the Permanganate Ion in Low-Temperature Frozen Matrices. *Inorg. Chem.* **2015**, *54*, 3370−3375.
(94) Retegan, M.; Krewald, V.; Mamedov, F.; Neese, F.; Lubitz, W.; Cox, N.; Pantazis, D. A. A five-coordinate Mn(iv) intermediate in biological water oxidation: spectroscopic signature and a pivot mechanism for water binding. *Chemical Science* **2016**, *7*, 72−84.
(95) Evans, D. H.; et al. Two-Electron Reactions in Organic and Organometallic Electrochemistry. *Acta Chem. Scand.* **1999**, *53*, 765−774.
(96) Kusunoki, M. S1-state Mn4Ca complex of Photosystem II exists in equilibrium between the two most-stable isomeric substates: XRD and EXAFS evidence. *J. Photochem. Photobiol., B* **2011**, *104*, 100−110.
(97) Rapatskiy, L.; Cox, N.; Savitsky, A.; Ames, W. M.; Sander, J.; Nowaczyk, M. M.; Rögner, M.; Boussac, A.; Neese, F.; Messinger, J.; Lubitz, W. Detection of the Water-Binding Sites of the Oxygen-Evolving Complex of Photosystem II Using W-Band 17O Electron−Electron Double Resonance-Detected NMR Spectroscopy. *J. Am. Chem. Soc.* **2012**, *134*, 16619−16634.
(98) Pérez Navarro, M.; Ames, W. M.; Nilsson, H.; Lohmiller, T.; Pantazis, D. A.; Rapatskiy, L.; Nowaczyk, M. M.; Neese, F.; Boussac, A.; Messinger, J.; Lubitz, W.; Cox, N. Ammonia binding to the oxygen-evolving complex of photosystem II identifies the solvent-exchangeable oxygen bridge (μ-oxo) of the manganese tetramer. *Proc. Natl. Acad. Sci. U. S. A.* **2013**, *110*, 15561−15566.

DOI: 10.1021/acs.inorgchem.6b03144
Inorg. Chem. 2017, 56, 4435−4445